university of groningen

University Medical Center Groningen

University of Groningen

Computational model of dot-pattern selective cells

Kruizinga, P.; Petkov, N.

Published in:
Biological Cybernetics

IMPORTANT NOTE: You are advised to consult the publisher's version (publisher's PDF) if you wish to cite from it. Please check the document version below.

Document Version
Publisher's PDF, also known as Version of record

Publication date:
2000

Link to publication in University of Groningen/UMCG research database

Citation for published version (APA):
Kruizinga, P., & Petkov, N. (2000). Computational model of dot-pattern selective cells. *Biological Cybernetics*, *83*(4), 313-325.

Copyright
Other than for strictly personal use, it is not permitted to download or to forward/distribute the text or part of it without the consent of the author(s) and/or copyright holder(s), unless the work is under an open content license (like Creative Commons).

The publication may also be distributed here under the terms of Article 25fa of the Dutch Copyright Act, indicated by the “Taverne” license. More information can be found on the University of Groningen website: https://www.rug.nl/library/open-access/self-archiving-pure/taverne-amendment.

Take-down policy
If you believe that this document breaches copyright please contact us providing details, and we will remove access to the work immediately and investigate your claim.

Downloaded from the University of Groningen/UMCG research database (Pure): http://www.rug.nl/research/portal. For technical reasons the number of authors shown on this cover page is limited to 10 maximum.

Download date: 06-05-2023

Biol. Cybern. 83, 313–325 (2000)

Biological Cybernetics
© Springer-Verlag 2000

Computational model of dot-pattern selective cells

P. Kruizinga, N. Petkov

Institute of Mathematics and Computing Science, University of Groningen, P.O. Box 800, 9700 AV Groningen, The Netherlands

Received: 20 December 1999 / Accepted in revised form: 3 March 2000

Abstract. A computational model of a dot-pattern selective neuron is proposed. This type of neuron is found in the inferotemporal cortex of monkeys. It responds strongly to groups of dots and spots of light intensity variation but very weakly or not at all to single dots and spots that are not part of a pattern. This non-linear behaviour is quite different from the spatial frequency filtering behaviour exhibited by other neurons that react to spot-shaped stimuli, such as neurons with centre-surround receptive field profiles found in the lateral geniculate nuclei and layer $4C\beta$ of V1. It is implemented in the proposed computational model by using an AND-type non-linearity to combine the responses of centre-surround cells. The proposed model is capable of explaining the results of neurophysiological experiments as well as certain psychophysical observations.

1 Introduction

Von der Heydt et al. (1991, 1992) reported on the properties of a specific type of orientation selective neuron in areas V1 and V2 of the visual cortex of monkeys that they called the *grating cell*. Similarly to other orientation selective neurons, such as simple, complex and hyper-complex cells, grating cells respond vigorously to a grating of bars of appropriate orientation, position and periodicity. In contrast to other orientation selective cells, grating cells respond very weakly or not at all to single bars, that is, bars that are isolated and are not part of a grating. This behaviour of grating cells cannot be explained by linear filtering followed by half-wave rectification as in the case of simple cells (Movshon et al. 1978b; Andrews and Pollen 1979; Maffei et al. 1979; Glezer et al. 1980; Kulikowski and Bishop 1981), nor by three-stage models of the type used for complex cells (Movshon et al. 1978a; Spitzer and Hochstein 1985; Morrone and Burr 1988). The non-linear processing properties of grating cells were reproduced by a computational model based on an AND-type non-linear combination of the responses of a group of simple cells (Kruizinga and Petkov 1995, 1999; Petkov and Kruizinga 1997; Kruizinga 1999).

Tanaka et al. (1991) found cells in the inferotemporal cortex that were maximally activated by dot patterns. These cells belonged to a larger group of cells that they called 'texture cells'. The majority of these texture cells responded optimally to gratings, and the description of the cells fully complies with the description of the grating cells given by Von der Heydt et al. (1992).

The cells found by Tanaka et al. (1991) seem to have characteristics similar to grating cells. They maximally react to a pattern that consists of a number of dots, though they are also excited by grating patterns, although to a considerably less extent. The neurophysiological experiments revealed a preference of the cells for regular dot patterns over more random patterns of dots. The cells are selective for the polarity of the stimulus: cells that strongly react to a pattern of white dots on a black background showed no reaction to patterns of black dots on a white background. Finally, it was reported that the exact shape of the texture elements (squares vs dots) was not critical. We call these neurons *dot-pattern selective cells*.

The role of these dot-pattern selective cells seems to be similar to the role of the grating cells: they detect areas in the visual field that contain texture that is built of specific texture elements. This behaviour can be explained by a model in which responses to individual texture elements are combined to produce a response to a pattern of such elements.

Since dot-pattern selective cells and grating cells seem to play similar roles, namely to detect a particular class of texture, the model of dot-pattern selective cells that is proposed here is in a way analogous to the model of grating cells: first individual texture elements are detected. In this case, the elements are dots or, more generally, spots of light intensity variation in the visual field. Next, the responses to a small number of individual dots

Correspondence to: N. Petkov (e-mail: petkov@cs.rug.nl)

or spots are combined into one response of a subunit referred to as a spot-group subunit. Finally, the responses of the subunits in a certain neighbourhood are summed together to produce the response of a dot-pattern selective cell.

The parameters of the dot-pattern selective cell model differ from the parameters of the model of grating cells. Instead of a preferred orientation and spatial frequency, as with the grating cell model, the dot-pattern selective cell model has as parameters the dot size and the density of the dot distribution. Although there is no neurophysiological evidence yet, we hypothesise that the response of dot-pattern selective cells does not depend on the contrast of the stimulus. In the computational model this is accounted for by adopting the same type of contrast normalisation as used in the grating cell model (Petkov and Kruizinga 1997).

The article is organised as follows: in Sect. 2, we present a computational scheme for selective detection of intensity spots. In Sect. 3, a model of dot-pattern selective cells is presented and a number of computational experiments are carried out to validate the model. Section 4 describes the evaluation of the texture discrimination properties of the model by means of the Mahalanobis distance. A comparison is made with some texture operators that are widely used in computer vision. In Sect. 5, a further comparison is made on the basis of the results of segmentation experiments. In the last section, the results are summarised and some conclusions are drawn concerning the role of the dot-pattern selective cell in visual information processing.

2 Detectors of intensity spots

Though most of the cells in the primary visual cortex (area V1) are orientation selective, about 10–20% of them do not show any orientation preference. They are called *unoriented* or *broadband* cells. The majority of these cells are found in layer $4C\beta$ of V1 and in the so-called cytochrome oxidase blobs (Blasdel and Fitzpatrick 1984; Livingstone and Hubel 1984; Ts'o and Gilbert 1988). Most of them resemble lateral geniculate nucleus (LGN) cells in that they have a centre-surround receptive field profile, although some unoriented cells have no inhibitory surround region. Centre-surround receptive field profiles can be modelled by means of a difference of Gaussian (DoG) impulse response function (Fig. 1)

$$u_{\xi,\eta,\sigma,\gamma}(x,y) = \frac{1}{2\pi\sigma^2}\left(\frac{1}{\gamma^2}\mathrm{e}^{-\frac{(x-\xi)^2+(y-\eta)^2}{2\gamma^2\sigma^2}} - \mathrm{e}^{-\frac{(x-\xi)^2+(y-\eta)^2}{2\sigma^2}}\right) \quad (1)$$

where the image point coordinates x and y specify the position of a light impulse in the visual field and ξ, η, σ, and γ are parameters explained in more detail below.

The centre of the receptive field within the visual field is specified by the pair (ξ, η). The parameters σ and γ specify the standard deviations $\sigma_c = \gamma\sigma\,(\gamma < 1.0)$ and $\sigma_s = \sigma$ of the centre and the surround Gaussians, respectively. In our experiments, we used a value of $\gamma = 0.5$, which is in accordance with the experimental

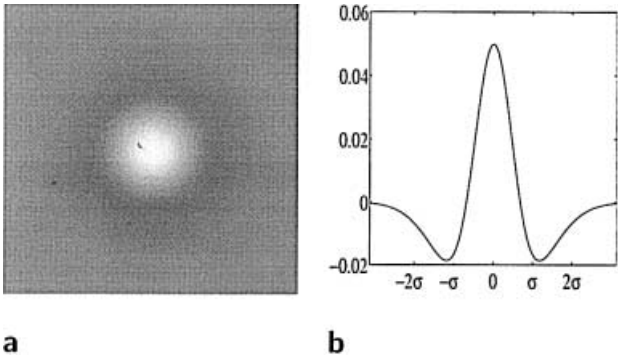

Fig. 1. A two-dimensional difference of Gaussian function: **a** intensity map, and **b** one-dimensional profile along a line through the centre of symmetry

data obtained by Kingdom et al. (1997). The normalisation factor $1/\gamma^2$ in front of the centre Gaussian is used to obtain a function with a zero DC component, which is also in agreement with neurophysiological data. With this value of the parameter γ, the radius of the centre region is the following function of σ:

$$r_\sigma = 0.96\sigma \ . \quad (2)$$

In our experiments, we use two types of such functions: one with a positive (excitatory), and the other with a negative (inhibitory) central region. Following tradition, they are referred to as 'centre-on' and 'centre-off' receptive field functions. The former is defined by (1), the latter differs from it only by a factor of -1.

The response of the concerned type of cell is modelled by a two-stage model: first a linear spatial summation stage and second, a non-linear stage that includes contrast normalisation and thresholding.

The linear stage consists in computing an integral:

$$s_{\xi,\eta,\sigma,\gamma} = \iint f(x,y)u_{\xi,\eta,\sigma,\gamma}(x,y)\mathrm{d}x\,\mathrm{d}y \quad (3)$$

where $f(x,y)$ is the light intensity distribution in an input image.

A contrast normalisation mechanism follows, to ensure that the detection of features is more or less independent of their contrast (Dean 1981; Ohzawa et al. 1982). Although we did not find evidence for this mechanism in the neurophysiological literature, we hypothesise that contrast normalisation will also take place in analogy with other types of visual neurons, for example, simple cells. Contrast normalisation is performed by dividing the quantity $s_{\xi,\eta,\sigma,\gamma}$ by the average gray level $a_{\xi,\eta,\sigma}$ of the image within the concerned receptive field; the latter is computed as follows, using the 'surround' Gaussian as a weighting function:

$$a_{\xi,\eta,\sigma} = \frac{1}{2\pi\sigma^2}\iint f(x,y)\mathrm{e}^{-\frac{(x-\xi)^2+(y-\eta)^2}{2\sigma^2}}\mathrm{d}x\,\mathrm{d}y \quad (4)$$

The ratio

$$l_{\xi,\eta,\sigma,\gamma} = \frac{s_{\xi,\eta,\sigma,\gamma}}{a_{\xi,\eta,\sigma}} \quad (5)$$

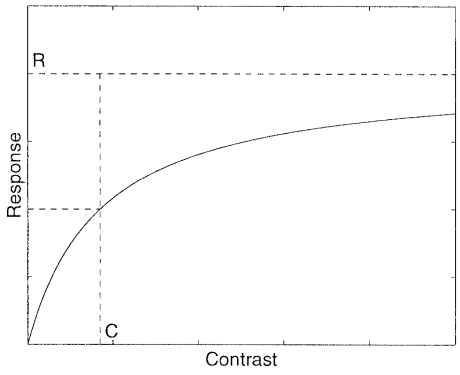

Fig. 2. The hyperbolic ratio function used for thresholding and contrast normalisation

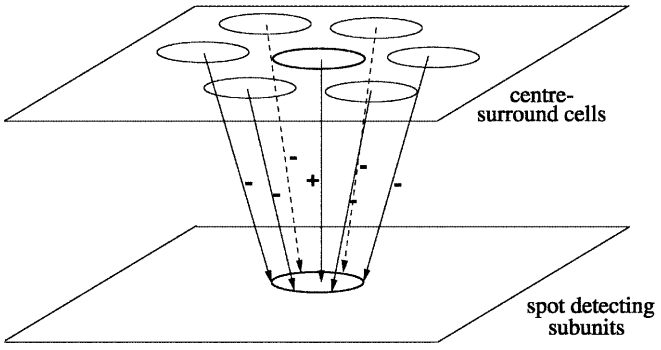

Fig. 3. A group of centre-surround cells provide excitatory and inhibitory input to a spot-detecting subunit. The cells are represented by the central regions of their receptive fields. The layered structure is for illustration purposes only

is proportional to the local contrast within the receptive field. Finally, the response $v_{\xi,\eta,\sigma,\gamma}$ of the concerned modelled cell is computed as the hyperbolic ratio function from the local contrast ratio $l_{\xi,\eta,\sigma,\gamma}$ (Albrecht and Hamilton 1982; Sclar et al. 1990):

$$v_{\xi,\eta,\sigma,\gamma} = \begin{cases} 0 & \text{if } a_{\xi,\eta,\sigma} = 0 \\ \chi\left(\frac{l_{\xi,\eta,\sigma,\gamma}\mathrm{R}}{l_{\xi,\eta,\sigma,\gamma}+\mathrm{C}}\right) & \text{otherwise} \end{cases} . \tag{6}$$

where $\chi(z) = 0$ for $z < 0$, $\chi(z) = z$ for $z \geq 0$ (thresholding), and R and C are constants that represent the maximum response and the semi-saturation level, respectively (Fig. 2).

An unoriented cell modelled by a centre-on receptive field function will react strongly to a light spot that is located entirely in the centre, excitatory region of the receptive field. In contrast, a centre-off cell will react to a dark spot on a light background. Both types of cells will also react to other features in their receptive fields such as lines or edges. The function of an ideal spot detector is, however, to signal spots only. Our computational model of such an ideal spot detector is based on a lateral inhibition mechanism. A spot-detecting subunit whose response will be denoted by $v'_{\xi,\eta,\sigma,\gamma}$ gets as positive input the output $v_{\xi,\eta,\sigma,\gamma}$ of a centre-surround cell centred on position (ξ,η) and as negative input the output of a number of other centre-surround cells with the same preferred spot size but with the centres of their receptive fields located in the vicinity of (ξ,η) (Fig. 3). The distance $\mathrm{R_{lat}}$ between the centres of the receptive fields of the cells that provide inhibitory input to the concerned subunit and the centre of the receptive field of the cell that provides excitatory input is chosen in such a way that the response of the subunit is equal to the response of the latter cell if a spot of the size of the central region of that cell is present. This is the case for $\mathrm{R_{lat}} = 1.36\sigma$. In this case, an optimal spot stimulus with a size exactly equal to the size of the central region of the receptive field will induce no response in the concerned surrounding cells that provide an inhibitory input to the subunit. We use the term 'subunit', not 'cell', on purpose. The concept of a spot-detecting subunit is introduced to represent a given step in our computational model and not to suggest the existence of a special type of cell with such a function. Even the assumption that the role of such a subunit is fulfilled by a dendrite of a dot-pattern selective cell would be overly speculative.

Other image features, such as edges and bars, may also invoke a reaction of the concerned centre-surround cell, but they will cause a reaction of the involved nearby cells as well. In that case, the output of the spot-detecting subunit $v'_{\xi,\eta,\sigma,\gamma}$ is influenced by the outputs of the nearby centre-surround cells, in such a way that if at least one of these cells is active, the subunit response is suppressed. In our model, the lateral inhibition scheme involves a fixed number of nearby centre-surround cells whose receptive field centres lie on a circle of radius $\mathrm{R_{lat}}$ around the centre (ξ,η) of the receptive field:

$$v'_{\xi,\eta,\sigma,\gamma} = \begin{cases} v_{\xi,\eta,\sigma,\gamma} & \text{if } \forall i, i \in \{1 \ldots N\}, \\ & \quad v_{\xi+\Delta\xi_i,\eta+\Delta\eta_i,\sigma,\gamma} < \rho v_{\xi,\eta,\sigma,\gamma} \\ 0 & \text{otherwise} \end{cases} \tag{7}$$

$$\Delta\xi_i = \mathrm{R_{lat}} \cos\left(\frac{2\pi i}{N}\right), \quad \Delta\eta_i = \mathrm{R_{lat}} \sin\left(\frac{2\pi i}{N}\right) \tag{8}$$

where ρ is a fixed factor – in our experiments we used $\rho = 0.8$. The number of nearby cells that are involved in the inhibition process is set to $N = 15$. This value is high enough to guarantee that the spot-detecting subunits do not react to features other than spots.

In our experiments, we use spot-detecting subunits with different values of σ to achieve the detection of spots of different sizes. This introduces a coding redundancy since spot-detecting subunits on more than one scale, with the receptive fields centred at the same position, will react to a spot in their receptive field. Beside the spot-detecting subunit with the appropriate size of the centre region, all subunits centred on the same position will show a response. This redundancy can be eliminated by suppressing all non-optimal responses. This is implemented by a winner-takes-all mechanism across all subunits with the same receptive field centre position but with different values of the size parameter σ. The ultimate response of a spot-detecting subunit $\tilde{v}_{\xi,\eta,\sigma,\gamma}$ is computed as follows:

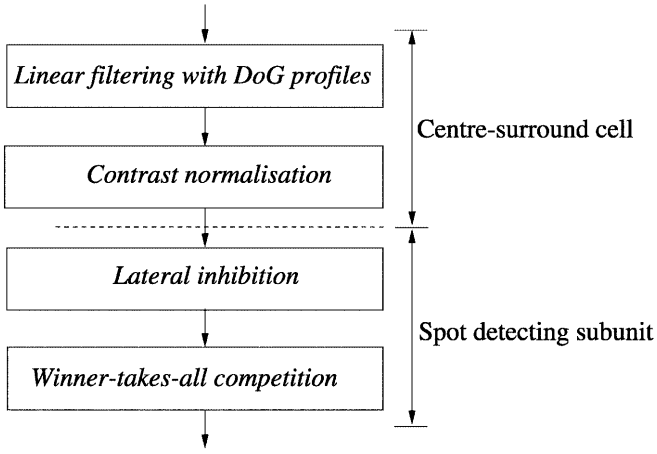

Fig. 4. A schematic overview of the stages in the models of centre-surround cells and spot-detecting subunits

$$\tilde{v}_{\xi,\eta,\sigma,\gamma} = \begin{cases} v'_{\xi,\eta,\sigma,\gamma} & \text{if } v'_{\xi,\eta,\sigma,\gamma} = \max\{v'_{\xi,\eta,\sigma',\gamma} \mid \forall \sigma'\} \\ 0 & \text{otherwise} \end{cases} \quad (9)$$

The winner-takes-all mechanism will cause the information concerning the location of spots in the image to be separated into different channels, depending on the size of the spots. The sensitivity to spots with different sizes therefore depends on the sampling of the scale range. In our experiments, we used four different scales.

The model presented above will detect spots of a specific size in the visual field, independent of the contrast and discarding other image features such as lines and edges. A schematic overview of the model is shown in Fig. 4 and the processing of visual information by this model is illustrated in Fig. 5, together with the results at intermediate stages. The intensity of a pixel in a result image represents the response of the corresponding part of the model with a receptive field centred at that pixel.

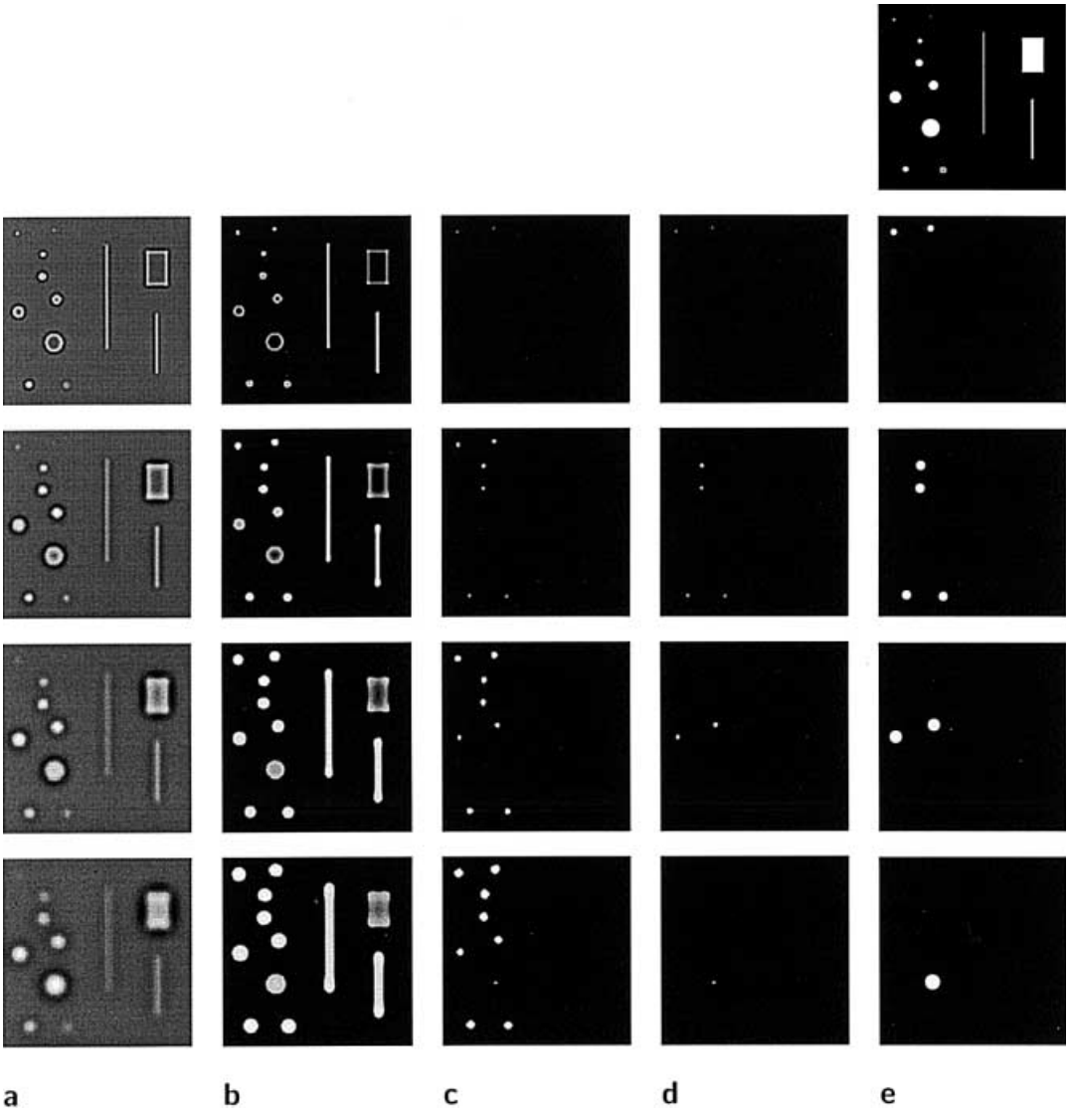

Fig. 5a–e. The single image in *top-right* position is a synthetic input image, which includes features of different form, size, and contrast. Each row in the 4×5 block of images corresponds to a given optimal size of the spots to be detected. **a** Results of convolutions with centre-surround receptive field functions of four different sizes. **b** The results normalised for contrast. The effect of lateral inhibition and winner-take-all competition on the responses of spot-detecting subunits are illustrated in **c** and **d**, respectively. For illustration purposes, in **e**, the responses of the spot-detecting subunits are replaced by the corresponding optimal size stimuli

As can be seen from the intermediate results after convolution of the input image with a centre-surround receptive field function (Fig. 5a), there is a response to spots, but also to other image features. At this stage, the strength of the response depends on the local contrast of the features. This dependence is eliminated by the contrast normalisation step (Fig. 5b). The lateral inhibition eliminates the response to non-spot stimuli (Fig. 5c). Finally, the winner-takes-all mechanism across all channels suppresses all responses to sub-optimal spot stimuli and ensures that a spot is detected in one channel only (Fig. 5d).

3 Dot-pattern selective cells

3.1 Computational model

The dot-pattern selective cell model is basically very similar to the model of grating cells (Petkov and Kruizinga 1997; Kruizinga and Petkov 1999). A dot-pattern selective cell receives input from spot-detecting subunits that are combined by an AND-type nonlinearity in such a way that modelled dot-pattern selective cells will only react if a number of spots of a specific size are detected in the receptive field of the cell. The response appears at a given minimum number of spots, then rises with the number of additional spots up to a given maximum and finally flattens out. This model of dot-pattern selective cells is next explained in more detail.

The activity of a so-called spot-group subunit, $t_{\xi,\eta,\sigma,\gamma,\zeta}$, with position (ξ,η) and preferred spot size specified by (2), is computed as follows (Fig. 6):

$$t_{\xi,\eta,\sigma,\gamma,\zeta} = \begin{cases} 1 \text{ if } \mathrm{Card}\{\tilde{v}_{\xi+\Delta\xi_i,\eta+\Delta\eta_i,\sigma,\gamma} : \tilde{v}_{\xi+\Delta\xi_i,\eta+\Delta\eta_i,\sigma,\gamma} > \Theta, \\ \qquad i \in [1 \ldots n]\} \geq m \\ 0 \text{ otherwise} \end{cases} \tag{10}$$

The above equation says that the response is 1 if the response of at least m out of $n\,(m < n)$ spot-detecting subunits exceeds a given threshold Θ. The positions $(\xi + \Delta\xi_i, \eta + \Delta\eta_i)$ of the concerned spot-detecting subunits are taken at random within the neighbourhood of (ξ,η):

$$\begin{aligned} \Delta\xi_i &= (\zeta + r_i) r_\sigma \cos\alpha_i \\ \Delta\eta_i &= (\zeta + r_i) r_\sigma \sin\alpha_i \quad (i = 1, \ldots, n) \end{aligned} \tag{11}$$

where ζ $(1.5 < \zeta)$ is a number that parametrises the density of the spots in the pattern, relative to their size, r_i are random numbers taken from a normal distribution with a zero mean and a standard deviation of 0.5 and α_i are random numbers taken from a uniform distribution between 0 and 2π. The number of locations n that are taken into account is larger than the minimum number m of spots to be detected. In our experiments, we set the number of inspected locations to $n = 30$ and the minimum number m of spots to be detected to $m = 3$. The spot-group subunit is activated only if three or more spots are detected in the inspected 30 locations. This is similar to the detection of oriented texture by grating subunits in the grating cell model (Petkov and Kruizinga 1997; Kruizinga and Petkov 1999). The difference between the models is the loose constraint for the positioning of the detected spots in the dot-pattern selective cell model: spots can be located at random positions within the receptive field, while in the case of the grating cell model the location of the bar primitives is more strictly determined to guarantee the detection of gratings with a specific preferred spatial-frequency.

The role of the spot-group subunit in the overall model of dot-pattern selective cells is to generate response to a group of structural elements, in this case spots, but remain silent to single elements.

In the final stage of the model of a dot-pattern selective neuron, its response $b_{\xi,\eta,\sigma,\gamma,\zeta}$ is computed by a weighted summation of the responses of spot-group subunits:

$$b_{\xi,\eta,\sigma,\gamma,\zeta} = \iint \mathrm{e}^{-\frac{(\xi-\xi')^2+(\eta-\eta')^2}{2\beta\sigma^2}} t_{\xi,\eta,\sigma,\gamma,\zeta}\,\mathrm{d}\xi'\,\mathrm{d}\eta' \tag{12}$$

This spatial summation is to provide that if more than m spots are encountered in the receptive field of the cell, the response will increase with the number of additional spots and will flatten out after reaching a certain maximum that is determined by the size of the receptive field. Again this mechanism is similar to the grating cell model in which the response of a grating cell is computed as a weighted summation of grating subunits.

The parameter β in (12) specifies the size of the region in which the weighted summation takes place and determines, together with the parameters σ and ζ, the effective size of the receptive field of the dot-pattern selective cell. Larger values of β result in a uniform response to a dot-pattern texture area even with larger discontinuities in the dot-pattern. The disadvantage, however, is an inaccuracy in determining the edges of the dot-pattern texture area or the transitions to areas with other spot statistics. The choice of this parameter in our model, $\beta = 8$, is an empirically determined balance between uniformity and accuracy.

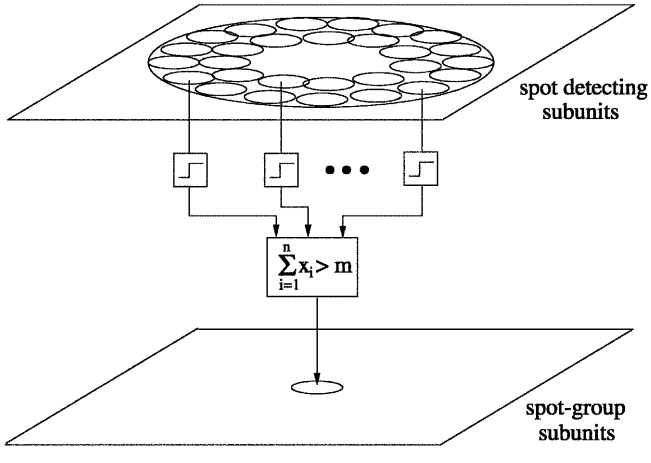

Fig. 6. A spot-group subunit is activated if at least m out of $n(m < n)$ spot-detecting subunits (taken at random positions) in its receptive field are active. The inputs to the spot-group subunit are first binarised. The layered structure is for illustration purposes only

3.2 Computer simulations with the dot-pattern selective cell model

To validate the model as described above, we carried out a number of computational experiments in which the model is applied to different visual stimuli. These stimuli were chosen to elicit characteristic responses of the modelled cells. Experiments were carried out with patterns of spots of different shape, size, contrast, and density, but also with isolated spots and non-spot stimuli like edges and lines.

Figure 7 shows the response of dot-pattern selective cells to patterns that consist of structure elements of the same size, contrast, and density but differ in the form of the structure elements (spot vs triangle). The response images in the bottom row show that the model is not sensitive to the exact form of the stimuli. The intensity of a pixel in a result image represents the activity of a modelled dot-pattern selective cell whose receptive field is centred on the concerned pixel. All responses that are represented in one such result image correspond to modelled dot-pattern selective cells with equal values of the model parameters except the values of the centre coordinates of their respective receptive fields. They are optimally tuned to dot patterns of a specific spot size, determined by the parameter σ of the model, and density of the spots in the pattern, determined by the product ζr_σ.

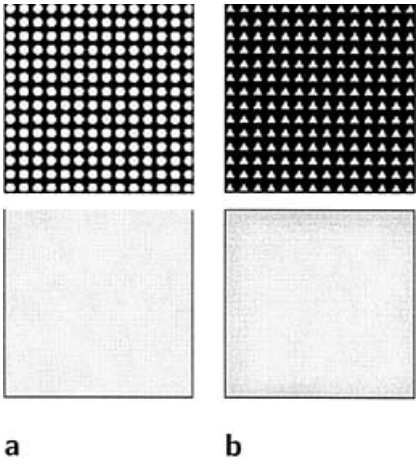

Fig. 7a, b. Input stimuli (*upper row*) and computed result images that correspond to the responses of modelled dot-pattern selective cells (*lower row*). Responses of the modelled cells to a pattern of spots with an optimal size and density **a** and to a pattern of structure elements (*triangles*) of the same size and density but of a different form **b**. The responses are high (as indicated by the light intensity in the result images) in both cases

The upper row of Fig. 8 shows a number of visual stimuli for which the response of modelled dot-pattern selective cells is computed; the results are shown in the lower row of images. Figure 8a shows a dot pattern that elicits maximal response from the model with given parameter values. The response drops to zero if the size of the spots is changed to a non-optimal value or when another spot density is used (Fig. 8b,c). The lower image in Fig. 8d shows the response to an input image (upper image) that contains a dot pattern that is an optimal stimulus with respect to the spot size and density, with spots of constant intensity on a background of increasing intensity. The Michelson contrast between the spots and the background varies, but as can be seen from the result image, this does not have an effect on the response of the dot-pattern selective cells within a broad range of contrast values (cf. Fig. 8a). When the contrast drops below a certain threshold, the spot-detecting subunits are not able to detect the spots, so that the subsequent spot-group subunits and finally the dot-pattern selective cells remain inactive as well.

Figure 9a shows an input image with non-spot image features (top row) and the response to these stimuli as computed with the dot-pattern selective cell model (bottom row). The model parameters (spot size and density) have the same values as in the experiments of Fig. 8. As can be seen from the results, the model does not react to image features other than spots.

Our hypothesis is that dot-pattern selective cells act in the same way as grating cells in that they extract higher-order statistics from an image by combining the inputs from a number of feature detectors. Since the underlying detectors have a preference for a specific type of feature, the cells will not react to other image features. The modelled cells also do not react to isolated features of the appropriate type, because of the AND-type

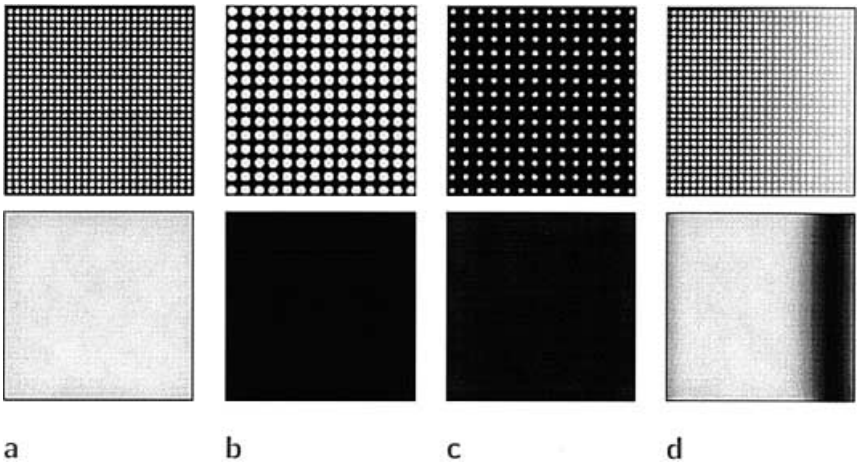

Fig. 8a–d. Input stimuli (*upper row*) and computed result images that correspond to the response of modelled dot-pattern selective cells (*lower row*); light and dark intensities mean strong and weak or no response, respectively. **a** Response of the modelled cells to a pattern of spots with an optimal size and density. Patterns with different spot size **b** or density **c** do not elicit any activity of the model. **d** The response is constant for a broad range of spot contrasts

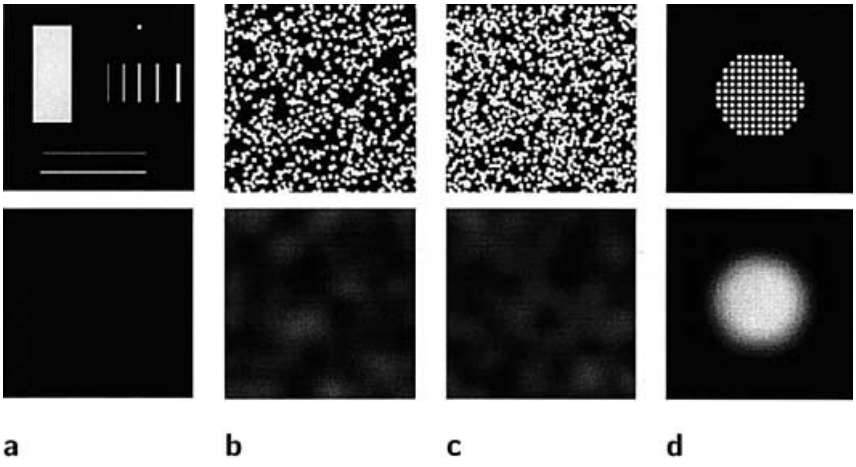

Fig. 9a–d. Input stimuli (*upper row*) and computed result images that correspond to dot-pattern selective cell responses (*lower row*). The modelled cells do not react to single dot stimuli and to non-spot image features as lines and edges **a**. Irregular dot patterns of optimal spot size and average density result in a response that is smaller than the response to a regular pattern **b** (cf. Fig. 8a). Even when the density of spots is increased, the response does not rise **c**. The detection capability of dot-pattern selective cells is illustrated in **d**: the cells react only in the area filled with a dot-pattern texture

non-linear mechanism employed to detect the presence of multiple features.

The response of the model to dot patterns with a random spot distribution is shown in Fig. 9b. The size of the spots is optimal and their density across the input image is the same as in the optimal case shown in Fig. 8a, which contains a regular (periodic) pattern. The response to this pattern is small though not zero. This is in agreement with the neurophysiological findings of Tanaka et al. (1991). They found that the cells that are optimally tuned to detect dot patterns in an image have a preference for regular patterns over irregular patterns. A surprising aspect of the model presented above is that this behaviour is not deliberately included in the model. The inputs from the spot-detecting subunits that are combined for the computation of the spot-group subunit response are taken from random positions around the centre of the receptive field. The small response of the model to a randomly ordered dot pattern is therefore not due to the underlying mechanism, but to the fact that a random distribution of the spots causes nearby spots to be glued together to form non-spot features, which prevents the spot-detecting subunits from reacting. At the same time, the gaps in the irregular pattern are larger than the ones in the regular pattern. When the number of spots in the image is increased (Fig. 9c), resulting in a smaller number of gaps, the response is still small. The fact that the response of the model to irregular dot patterns is smaller than the response to regular patterns should be considered as a qualitative property of the model. The difference can be attenuated by applying a sub-linear monotonously increasing function, such as logarithm or the hyperbolic ratio function (Fig. 2), to the output of the model.

The dot-pattern detection capabilities of the model are illustrated in Fig. 9d. Dot-pattern selective cells only react to dot patterns, discarding all other image features (cf. Fig. 9a and d). In this respect, dot-pattern selective cells are similar to grating cells that react to gratings of bars but do not react to simple bars or other features.

From the results of these computer simulations it may be concluded that the model presented in the previous section is capable of reproducing the main properties of this type of neuron as known from neurophysiological experiments.

3.3 Dot-pattern selective cells versus grating cells

The question may be due of what the added value of the dot-pattern selective cells is for visual information processing given the existence of grating cells: both types of cells react to texture that is built of structure elements. In the case of the grating cells, the structure elements are bars and the only constraint is that they appear in more or less periodic patterns. In contrast, dot-pattern selective cells react strongly to spot-like structure elements that can be randomly distributed. In many cases, both types of cells will react; especially textures with a strict periodic pattern of spots will trigger both grating and dot-pattern selective cells.

Grating cells detect periodic one-dimensional light intensity variations; this means they specifically react to intensity distributions that do not change in one direction while changing periodically in the perpendicular direction. Viewed in that light, it should be clear that there are textures that cannot be adequately processed by grating cells. For instance, grating cells will not react to intensity distributions that are periodic in both the direction of their preferred orientation and the perpendicular orientation, that is, true two-dimensional periodic light intensity variations, as for example checkerboard patterns (Von der Heydt et al. 1992). This fact evidently necessitates another type of texture processing cell, like the dot-pattern selective cell. Figure 10 shows the response of both grating cells and dot-pattern selective cells to a checkerboard stimulus. The modelled grating cells have a preferred vertical orientation and a preferred periodicity that coincides with the horizontal periodicity of the checkerboard. The modelled dot-pattern cells have a dot size and spreading preference that is optimal for the checkerboard shown.

Figure 11a shows two dot-pattern textures, each with a different spot size and random spot distribution. Figure 11b and c show the segmentation results that were obtained on the basis of feature vectors computed with

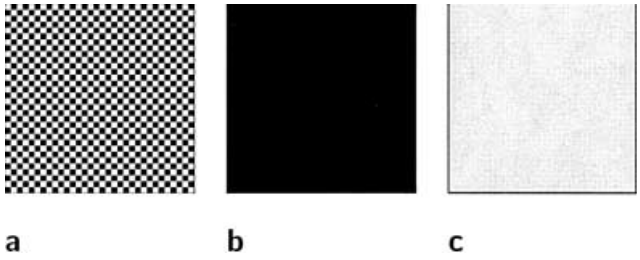

Fig. 10. **a** An input image of a checkerboard pattern and **b** the computed response image of grating cells with vertical preferred orientation and preferred periodicity equal to the periodicity of the checkerboard in horizontal orientation. The response image of optimally tuned dot-pattern selective cells is shown in **c**

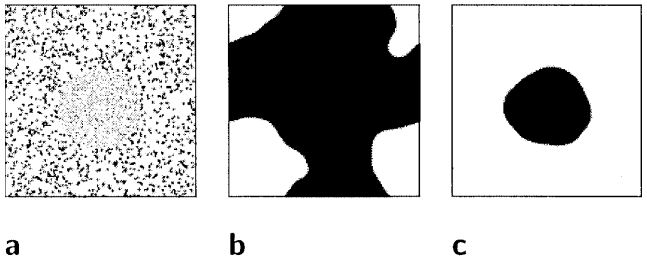

Fig. 11. **a** An input image containing two textures with randomly placed spots of different size and density, **b** the segmentation results obtained on the basis of the responses of the grating cell model, and **c** the dot-pattern selective cell model

the grating cell and the dot-pattern selective cell models, respectively. The results clearly show that the two textures that are present in the input image cannot be distinguished on the basis of the response of grating cells. The poor segmentation result is due to the fact that the response of grating cells to the concerned type of texture is negligible. Therefore, no adequate discrimination is possible. In contrast, the two textures can be separated using the responses of the modelled dot-pattern selective cell model. As was shown before, the response to a texture with randomly located spots is sub-optimal, but the dot-pattern selective cells still give a sufficient and rather uniform response within the two texture areas and a good separation can be made. This example illustrates the additional dimension that dot-pattern selective cells add to texture detection and discrimination.

The relation between grating cells and dot-pattern selective cells is further illustrated by a psychophysical experiment concerning the so-called Ouchi illusion. A simple pattern of two gratings with different orientations – a creation of the Japanese artist Ouchi – generates an illusion of relative motion (Fig.12a). To experience the motion illusion, look at the image at a distance of about 50 cm. The pattern in the inner disk seems to move as a whole, relative to the outer disk. Hine et al. (1995) have done a number of psychophysical experiments to reveal the exact conditions for the illusion to occur. Based on the results of these experiments they hypothesise that the illusion may be caused by grating cell activity. The fact that the pattern seems to move as a whole and especially the close match between the estimation of the orientation and spatial frequency bandwidth based on the illusion and on neurophysiological data (Von der Heydt et al. 1992) support this hypothesis.

The similar roles that grating cells and dot-pattern selective cells seem to play in texture processing suggests that this illusion will be experienced not only with a grating pattern, but also with dot patterns, at least as long as different classes of dot-pattern selective cells are activated by the patterns. Figure 12b shows such an illusion with dot patterns. As can be verified by the reader, a similar effect is observed indeed. Since the response of grating cells to this type of patterns is low, the effect may be due to the dot-pattern selective cells in the same way as grating cells may cause the original Ouchi illusion.

4 Texture discrimination properties of the dot-pattern selective cell operator

In this section, we look at the discrimination properties of a texture operator derived from the model of the dot pattern selective cell. To quantitatively measure the discrimination properties of this operator we compute the Mahalanobis distance between sets of feature vectors that are derived from different texture images. The

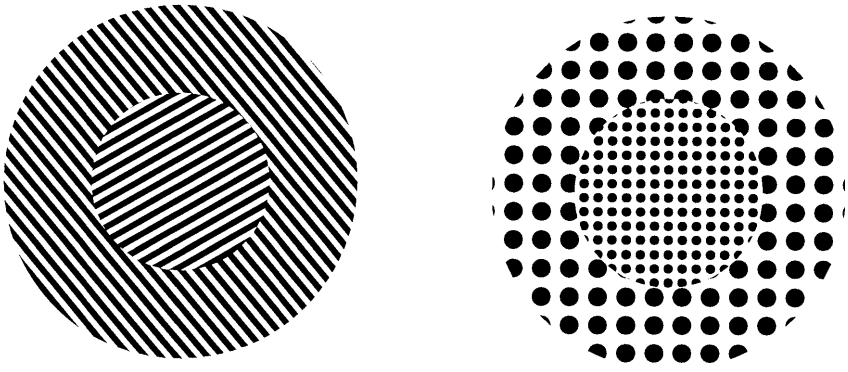

Fig. 12. The Ouchi illusion, with **a** grating patterns and **b** a similar illusion with dot patterns. The effect is enhanced by jiggling the pattern while looking at it (see Hine et al. 1995, 1997)

Mahalanobis distance (Mahalanobis 1936) between two sets of feature vectors is defined as follows:

$$D = \sqrt{(\boldsymbol{\mu}_1 - \boldsymbol{\mu}_2)\Sigma^{-1}(\boldsymbol{\mu}_1 - \boldsymbol{\mu}_2)} \tag{13}$$

where $\boldsymbol{\mu}_1$ and $\boldsymbol{\mu}_2$ are the mean vectors of the two sets and Σ^{-1} is their pooled covariance matrix.

It is closely related to Fisher's linear discriminant and Fisher's criterion (Fisher 1923). Fisher's linear discriminant function is a projection of the multidimensional feature space on a one-dimensional subspace, a line, such that the quantity

$$f = \frac{|\eta_1 - \eta_2|}{\sqrt{\sigma_1^2 + \sigma_2^2}} \tag{14}$$

which is called the Fisher criterion, is maximised. In (14), η_1 and η_2 are the projected means of the two sets of feature vectors and σ_1^2 and σ_2^2 are their respective variances. The relation between the maximum value of the Fisher criterion and the Mahalanobis distance is as follows:

$$D = \sqrt{2}f \tag{15}$$

The Mahalanobis distance thus quantifies the distance between two sets of feature vectors, relating it to their spatial spreading. Therefore, the larger the Mahalanobis distance, the larger the separability of the two concerned sets and the smaller their overlap. This property of the Mahalanobis distance gives the possibility to quantify the capability of a texture feature extraction operator to produce separable sets of feature vectors for different types of texture and to compare different operators.

We computed the Mahalanobis distance between pairs of sets of feature vectors extracted from nine different texture images shown in Fig. 13.

Since the dot-pattern selective cell operator is primarily suited for processing dot-pattern textures, the test set consists of images of this type. In a number of these texture images, the spots are arranged in a regular pattern. Other texture images have a more random distribution of the spots across the image. In the former case, not only the dot-pattern selective cell operator, but also the grating cell operator will respond, though its response will not be optimal. In the latter case, only the dot-pattern selective cell operator will respond, showing the role of the dot-pattern selective cell operator in the combination with the grating cell operator.

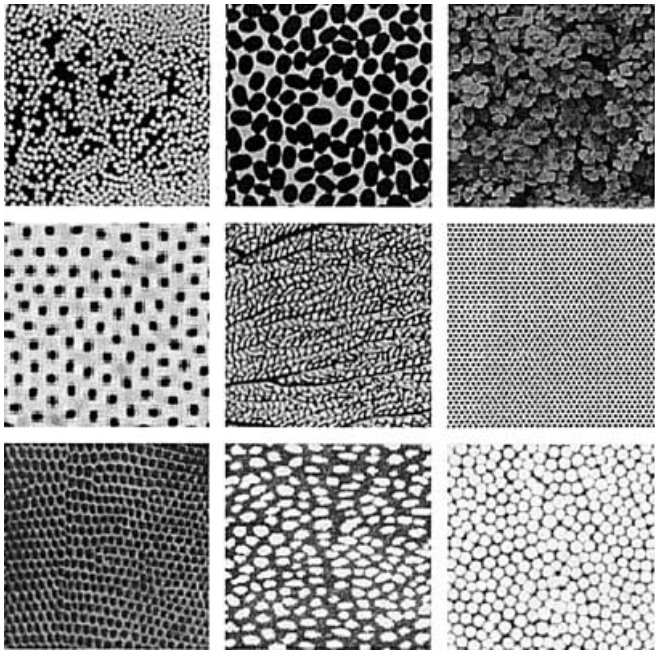

Fig. 13. Nine test images, denoted B1 through B9, left to right and top to bottom

As described elsewhere in more detail (Kruizinga and Petkov 1999), sets of feature vectors are obtained by applying a vector operator to each test image and taking 1,000 samples from each of the resulting vector fields. Similar to the experiments described in our previous work on texture operator comparison, 24-dimensional feature vector operators are used. In the case of the dot-pattern selective cell operator, this is achieved by a set of 24 different operators with four different spot sizes, three values for the spot density parameter ζ and for both black and white spots.

Table 1 lists the values of the Mahalanobis distance between sets of feature vectors computed with the dot-pattern selective cell operator. The values are all relatively high, with the lowest value being 7.74, which for two normally distributed sets of equal variance corresponds to an overlap of only 0.01%. This means that all pairs of test images can be linearly separated on the basis of the feature vectors obtained with a dot-pattern selective cell operator. The values are comparable with the values of the Mahalanobis distance obtained with the grating cell operator for pairs of oriented texture images

Table 1. Mahalanobis distance for features obtained with the dot-pattern selective cell operator

	B1	B2	B3	B4	B5	B6	B7	B8	B9
B1	–	22.22	14.67	52.40	7.74	25.33	11.96	11.26	22.16
B2		–	26.64	28.69	34.35	72.29	52.68	12.43	21.64
B3			–	65.82	10.15	33.56	17.66	11.48	22.84
B4				–	83.16	225.35	161.74	43.35	55.62
B5					–	43.37	11.62	15.46	30.89
B6						–	72.29	34.54	55.07
B7							–	25.72	43.18
B8								–	23.46
B9									–

Table 2. Mahalanobis distance for the Gabor-energy features

	B1	B2	B3	B4	B5	B6	B7	B8	B9
B1	–	3.20	6.09	7.41	3.01	27.05	7.09	5.03	2.79
B2		–	6.43	4.86	5.53	30.14	6.90	4.03	1.44
B3			–	7.72	7.34	38.57	4.84	7.64	7.28
B4				–	8.85	45.79	9.73	7.59	7.30
B5					–	23.15	8.43	6.63	5.57
B6						–	44.72	34.55	32.12
B7							–	8.02	8.34
B8								–	4.47
B9									–

Table 3. The Mahalanobis distance for the co-occurrence matrix features

	B1	B2	B3	B4	B5	B6	B7	B8	B9
B1	–	3.75	4.65	5.59	3.39	8.39	5.71	4.55	4.07
B2		–	5.35	4.62	6.51	8.19	5.94	4.03	4.60
B3			–	5.57	5.47	8.33	4.03	5.67	6.18
B4				–	7.76	8.79	5.78	6.10	6.73
B5					–	8.16	6.41	6.43	7.34
B6						–	8.58	8.97	8.46
B7							–	6.72	6.92
B8								–	5.73
B9									–

(see Kruizinga and Petkov 1999). The performance of the dot-pattern selective cell operator in segmentation tasks with dot-pattern textures can therefore be expected to be as good as the performance of the grating cell operator with respect to oriented texture.

Table 2 shows the values of the Mahalanobis distance for pairs of sets of feature vectors computed with the Gabor-energy operator (see Kruizinga and Petkov 1999). All values listed in this table are considerably smaller than the ones obtained with the dot-pattern selective cell operator. The minimum value is 1.44: this corresponds to an overlap of 48% of two normally distributed sets of equal variance, which means that the concerned vector sets cannot be separated by a linear discriminator. On average the Mahalanobis distance values are more than three times smaller than the values obtained with the dot-pattern selective cell operator. Note that texture image B6 can be separated very well from the other images; the values of the Mahalanobis distance for all pairs in which B6 is involved are much higher than all other values. This is due to the oriented structure of the honeycomb pattern in the image. When the pairs in which B6 is involved are excluded, the average value falls to 6.19. This is considerably smaller than the average value of 33.66 obtained with the dot-pattern selective cell operator, excluding texture B6 from the experiments.

The values of the Mahalanobis distance obtained with the co-occurrence matrix operator are listed in Table 3 (for details on the particular type of operator used, see Kruizinga and Petkov 1999). With an average value of 6.19 the co-occurrence matrix operator definitely does not perform as well as the other two operators. Note again that the values for pairs including B6 are larger. The reason is that, similar to the other operators, the co-occurrence matrix operator has a preference for periodicity in the textures.

Table 4. Statistics of the Mahalanobis distances

Feature type	Avg	Min	Max
Co-occurrence matrix features	6.19	3.39	8.97
Gabor-energy features	12.49	1.44	45.79
Dot-pattern selective cell features	41.73	7.74	225.35

Table 4 lists the average, the minimum, and the maximum Mahalanobis distances that were measured using the three concerned operators. From this table it may be concluded that the dot-pattern selective cell operator is superior to both the Gabor-energy and the co-occurrence matrix operator with respect to dot-pattern textures. For such textures, the specialised dot-pattern selective cell operator outperforms the general purpose texture operators.

5 Classification results comparison with other texture operators

In this section, the properties of the dot-pattern selective cell operator are further analysed by carrying out a classification results comparison. In this method a segmentation algorithm is applied to a feature vector field computed with the operator, and the segmentation performance and suitability of the used features are evaluated by using the number of misclassified pixels (Weszka et al. 1976; Conners and Harlow 1980; Pichler et al. 1996). In this way, the practical value of the operator can be evaluated and compared with other texture operators.

For this purpose a number of texture segmentation experiments were carried out in the following way. First a given texture operator is applied to an image that contains two or more different textures. The concerned

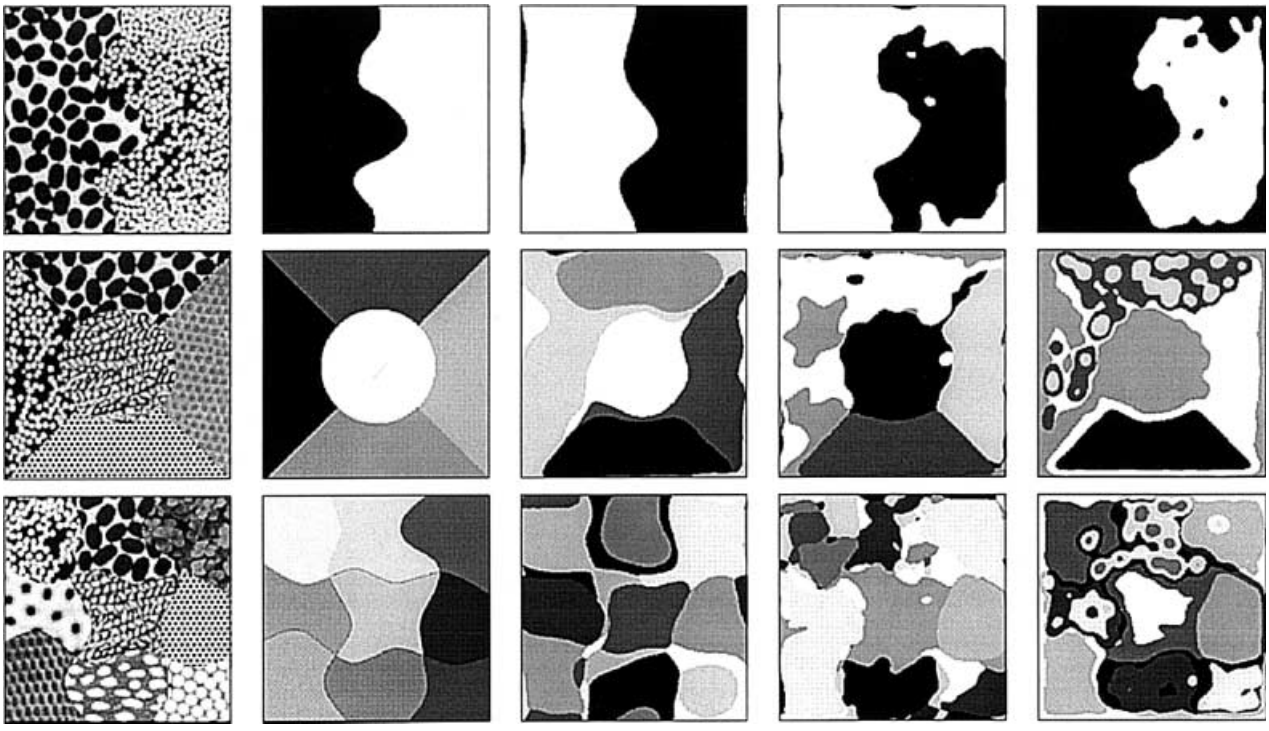

Fig. 14. Results of segmentation experiments using the K-means clustering algorithm. The *left-most column* shows three input images containing two, five, and nine textures. The *second column* shows the exact (manual) segmentation of the input images (the so-called ground truth); one grey level is used to mark the pixels that belong to one class. The *three right-most columns* show the segmentation results (using $K = 2$, $K = 5$, and $K = 9$ for the respective rows) based on the dot-pattern selective cell operator (*middle column*), the Gabor-energy operator, (*second column from the right*) and the co-occurrence matrix operator (*right-most column*)

operator is actually a vector operator in that it consists of a set of operators with different parameter settings (spot size and density). The resulting feature vector field is then used as an input to a general-purpose clustering algorithm that assigns individual vectors to clusters in the feature space. As in the case of a similar comparison of the grating cell operator with other operators presented elsewhere (Kruizinga and Petkov 1999), a K-means clustering algorithm is used for this purpose. This algorithm assigns the input feature vectors to a predetermined number of clusters K.

Three experiments were carried out, in which images containing an increasing number of textures had to be segmented. The results of these experiments are shown in Fig. 14. The leftmost column shows the input images that were used, with two, five and nine different textures, respectively. The second column from the left shows the perfect segmentations of the input images into regions of different texture. The other three columns show the results of the segmentation of the input images on the basis of the vector fields obtained with the three concerned texture operators: the dot-pattern selective cell operator, the Gabor-energy operator, and the co-occurrence matrix operator, respectively.

The segmentation results based on clustering of feature vectors obtained with the dot-pattern selective cell operator are reasonably good. The K regions, which result from the clustering by the K-means algorithm, correspond to the K regions in the input image that contain different textures. The only misclassified pixels are located at the borders of the texture regions; that is, there are no subregions inside a texture region that are not classified correctly. In comparison to the experiments concerning the application of the grating cell operator to oriented texture images (Kruizinga 1999; Kruizinga and Petkov 1999), a larger number of pixels are misclassified at the borders of the texture regions. This means that the dot-pattern selective cell operator is more sensitive to border effects in the estimation of the feature vectors in comparison to the grating cell operator.

The results obtained with the Gabor-energy operator are shown in the second column from the right. It is clear that in all three cases the segmentation is not as good as with the dot-pattern selective cell operator. In particular, the misclassification of pixels within a texture region and, in some cases, the inability to distinguish distinct textures are evident drawbacks. The results show the same characteristic as in the case of the segmentation of oriented texture based on the Gabor-energy features (Kruizinga and Petkov 1999): the segmentation performance decreases significantly when a larger number of different textures are involved.

The rightmost column shows the segmentation results based on the classification of the co-occurrence matrix feature vectors. The results are comparable with those of the Gabor-energy operator in that not all texture regions are classified correctly and that different parts of a

homogeneous texture region are assigned to different classes.

In conclusion, the results of the segmentation experiments confirm the outcome of the operator comparison on the basis of the Mahalanobis distance: with respect to dot-pattern textures, the dot-pattern selective cell operator clearly has better discrimination and segmentation properties than the other two operators.

6 Summary and conclusions

In this article, we introduced a computational model of dot-pattern selective cells. The model highly resembles the model of grating cells, as proposed elsewhere (Petkov and Kruizinga 1997), in that it employs an AND-type non-linearity for combining the inputs from subunits that detect structural elements. The parameters of the model include spot size and density. The model is capable of mimicking the main response properties of the dot-pattern selective cells as known from neurophysiological experiments.

Besides the similar roles dot-pattern selective cells and grating cells seem to play in visual information processing, they also respond in a similar way to certain visual stimuli. In particular highly periodic dot-pattern textures will trigger a response in both types of cells. Nevertheless, both grating cells and dot-pattern selective cells seem to be needed to cover the wide spectrum of textures that occur in nature. The computational experiments with textures with randomly positioned spots have clearly shown that there are situations in which grating cells fail to detect and discriminate texture while dot-pattern selective cells adequately solve these tasks.

To evaluate the discrimination properties of the texture operator derived from the model of dot-pattern selective cells, it was applied to a set of test images and for each pair of images the Mahalanobis distance was computed between the corresponding sets of feature vectors. A test set of dot-pattern textures was used. The resulting values of the Mahalanobis distance show that the proposed operator has excellent discrimination properties with respect to dot-pattern textures. Using the same test images, the Mahalanobis distances were computed for two other texture operators, namely the co-occurrence matrix operator and the Gabor-energy operator. The results clearly show that these operators are less well suited for dot-pattern texture processing than the dot-pattern selective cell operator.

A number of segmentation experiments were carried out to compare the dot-pattern selective cell operator with the other two texture operators with respect to their practical value in segmentation tasks. The three operators were applied to three test images containing an increasing number of dot-pattern textures. The general purpose K-means clustering algorithm was applied to the resulting feature vector fields to classify the individual feature vectors in K classes. The results confirm the superiority of the dot-pattern selective cell operator in comparison to the other two texture operators. Using this operator, the only misclassified pixels are located near the borders of the texture regions, whereas with the other operators entire subregions within the same texture are incorrectly classified.

Von der Heydt et al. (1992) put forward the hypothesis that grating cells might be an efficient means for quick preattentive identification of texture of vital importance for an animal, such as grass or a bunch of bananas. Petkov and Kruizinga (1997) demonstrated by means of computer experiments that grating cells can play an important role in the separation of form information, as coded in the contours of objects, from texture information, in particular in cases in which oriented texture is concerned.

Dot-pattern selective cells might play a similar role with respect to texture types other than oriented texture. While grating cells will react strongly to oriented texture such as grass or long leaves, dot-pattern selective cells will most strongly react to texture that consists of spots. Such texture is richly available in nature: think, for instance, of the rounded leaves of many plants, trees, and flowers.

Where grating cells are specialised in the processing of oriented texture, dot-pattern selective cells are specialised in the processing of dot-pattern textures. By employing different types of texture-processing cells, each specialised in the detection and analysis of a specific type of texture, the visual system is capable of accurately discriminating textures in visual scenes and separating texture from form. This strategy can also be adopted for texture analysis in artificial vision systems. Specialised operators perform substantially better than general purpose texture operators, at least with respect to their special domain.

References

Albrecht D, Hamilton D (1982) Striate cortex of monkey and cat: contrast response function. J Neurophysiol 48: 217–237

Andrews B, Pollen D (1979) Relationship between spatial frequency selectivity and receptive field profile of simple cells. J Physiol (Lond) 287: 163–176

Blasdel G, Fitzpatrick D (1984) Physiological organization of layer 4 in macaque striate cortex. J Neurosci 4: 880–895

Conners R, Harlow C (1980) A theoretical comparison of texture algorithms. IEEE Trans Pattern Anal Mach Intell 2: 204–222

Dean A (1981) The relationship between response amplitude and contrast for cat striate cortical neurons. J Physiol (Lond) 318: 413–427

Fisher A (1923) The mathematical theory of probabilities, vol 1. Macmillan, New York

Glezer V, Tsherbach T, Gauselman V, Bondarko V (1980) Linear and non-linear properties of simple and complex receptive fields in area 17 of the cat visual cortex. Biol Cybern 37: 195–208

Hine T, Cook M, Rogers G (1995) An illusion of relative motion dependent upon spatial frequency and orientation. Vision Res 35: 3093–3102

Hine T, Cook M, Rogers G (1997) The Ouchi illusion: an anomaly in the perception of rigid motion for limited spatial frequencies and angles. Percept Psychophys 59: 448–455

Kingdom F, McCourt M, Blakeslee B (1997) In defence of "lateral inhibition" as the underlying cause of induced brightness phenomena: a reply to Spehar, Gilchrist and Arend. Vision Res 37: 1039–1043

Kruizinga P (1999) Computational models of texture processing neurons. Ph.D. thesis, University of Groningen, The Netherlands

Kruizinga P, Petkov N (1995) A computational model of periodic-pattern-selective cells. Proceedings IWANN '95 (Lecture notes in computer science, vol 930). Springer, Berlin Heidelberg New York, pp 90–99

Kruizinga P, Petkov N (1999) Non-linear operator for oriented texture. IEEE Trans Image Process 8: 1395–1407

Kulikowski J, Bishop P (1981) Fourier analysis and spatial representation in the visual cortex. Experientia 37: 160–163

Livingstone M, Hubel D (1984) Anatomy and physiology of a color system in the primate visual cortex. J Neurosci 4: 309–356

Maffei L, Morrone M, Pirchio M, Sandini G (1979) Responses of visual cortical cells to periodic and non-periodic stimuli. J Physiol (Lond) 296: 27–47

Mahalanobis P (1936) On the generalized distance in statistics. Proc Natl Inst Sci Calcutta 12: 49–55

Morrone M, Burr D (1988) Feature detection in human vision: a phase-dependent energy model. Proc R Soc Lond B 235: 221–245

Movshon J, Thompson I, Tolhurst D (1978a) Receptive field organisation of complex cells in the cat's striate cortex. J Physiol (Lond) 283: 79–99

Movshon J, Thompson I, Tolhurst D (1978b) Spatial summation in the receptive fields of simple cells in the cat's striate cortex. J Physiol (Lond) 283: 53–77

Ohzawa I, Sclar G, Freeman R (1982) Contrast gain control in the cat visual cortex. Nature 298: 266–268

Petkov N, Kruizinga P (1997) Computational models of visual neurons specialised in the detection of periodic and aperiodic oriented visual stimuli: bar and grating cells. Biol Cybern 76: 83–96

Pichler O, Teuner A, Hosticka B (1996) A comparison of texture feature extraction using adaptive gabor filtering, pyramidal and tree structured wavelet transforms. Pattern Recogn 29: 733–742

Sclar G, Maunsell J, Lennie P (1990) Coding of image contrast in central visual pathways of the macaque monkey. Vision Res 30: 1–10

Spitzer H, Hochstein S (1985) A complex-cell receptive-field model. J Neurosci 53: 1266–1286

Tanaka K, Saito H, Fukada Y, Moriya M (1991) Coding visual images of objects in the inferotemporal cortex of the macaque monkey. J Neurophysiol 66: 170–189

Ts'o D, Gilbert C (1988) The organization of chromatic and spatial interactions in the primate striate cortex. J Neurosci 8: 1712–1727

Von der Heydt R, Peterhans E, Dürsteler M (1991) Grating cells in monkey visual cortex: coding texture? In: Blum B (ed) Channels in the visual nervous system: neurophysiology, psychophysics and models. Freund, London, pp 53–73

Von der Heydt R, Peterhans E, Dürsteler M (1992) Periodic-pattern-selective cells in monkey visual cortex. J Neurosci 12: 1416–1434

Weszka J, Dyer C, Rosenfeld A (1976) A comparative study of texture measures for terrain classification. IEEE Trans Sys Man Cybern 6: 269–285